Thermo-hydraulic characterization of a self-pumping corrugated wall heat exchanger

Kevin Schmidmayer, Prashant Kumar, Pascal Lavieille, Marc Miscevic, Frederic Topin

Energy 128 (2017) 713–728

Contents lists available at ScienceDirect

Energy

journal homepage: www.elsevier.com/locate/energy

Thermo-hydraulic characterization of a self-pumping corrugated wall heat exchanger

Kevin Schmidmayer [a, *], Prashant Kumar [a], Pascal Lavieille [b], Marc Miscevic [b], Frédéric Topin [a]

[a] Aix Marseille Univ, CNRS, IUSTI, 5, Rue Enrico Fermi, 13453 Marseille Cedex 13, France
[b] Laboratoire LAPLACE, CNRS UMR 5213, Université de Toulouse, 118, Route de Narbonne, 31062, Toulouse Cedex 9, France

ARTICLE INFO

Article history:
Received 2 January 2017
Received in revised form
18 March 2017
Accepted 10 April 2017
Available online 14 April 2017

Keywords:
Heat transfer enhancement
Wall morphing
Dynamic deformation
Pressure gain
Mobile heat exchanger

ABSTRACT

Compactness, efficiency and thermal control of the heat exchanger are of critical significance for many electronic industry applications. In this view, a new concept of heat exchanger at millimeter scale is proposed and numerically studied. It consists in dynamically deforming at least one of its walls by a progressive wave in order to create an active corrugated channel.

Systematic studies were performed in single-phase flow on the different deformation parameters that allow obtaining the thermo-hydraulic characteristics of the system. It has been observed the dynamic wall deformation induces a significant pumping effect. Intensification of heat transfer remains very important even for highly degraded waveforms although the pumping efficiency is reduced in this case.

The mechanical power applied on the upper wall to deform it dynamically is linked to the wave shape, amplitude, frequency and outlet-inlet pressure difference. The overall performance of the proposed system has been evaluated and compared to existing static channels. The performance of the proposed heat exchanger evolved in two steps for a given wall deformation. It declines slightly up to a critical value of mechanical power applied on the wall. When this critical value is exceeded, it deteriorates significantly, reaching the performance of existing conventional systems.

1. Introduction

Due to growing demands of energy in various industrial sectors, design and conception of heat exchanger devices are very crucial for performance of numerous energetic systems. Heat exchanger devices are present at various scales. Their applications can be found in large scale industries, e.g. power plants, to mini scale industries, e.g. electronic industries.

The temperature control and associated heat flux management is crucial in many applications: microelectronics, embedded or fixed power electronics systems, power station, air conditioners, heat pumps, as well as in the field of industrial thermal processes metallurgy, chemistry, food, etc. The will to increase the performance and efficiency of these systems greatly amplifies this need as, in many situations; it becomes the limiting factor in optimizing system performance. Moreover, lifetime and reliability of many systems are very strongly related to the quality of the thermal management.

This situation is clearly identified, for example, in power electronics where the electrical power passing through an elementary component could be increased by a factor 10 or more (thus reducing the number of elementary components) if the performance of cooling system allowed evacuating the produced heat flux (Mohan et al. [1]). Adding the fact that the main system mass is contained in the copper plate for the heat dissipation, and the fact that the planar architecture of the electronics is imposed by the cooling system, one understands the stakes in terms of compactness, performance and weight reduction.

It is nowadays common to meet chemical or thermal systems whose channels have sub-millimetric hydraulic diameters. This trend towards miniaturization is mainly due to the increasing demands of new and effective mixing or heat transfer technologies for various industrial fields, associated to the increasing need to control highly exothermic or explosive chemical reactions (Kandlikar [2,3]).

If these systems can improve the compactness, one major

* Corresponding author.
E-mail address: kevin.schmidmayer@univ-amu.fr (K. Schmidmayer).

http://dx.doi.org/10.1016/j.energy.2017.04.048
0360-5442/

drawback is the difficulty to disturb the boundary layers as flow is mostly laminar in such small devices. Consequently, the net gain in terms of mass or heat transfer is principally due to the increase in the exchange surface per unit of volume. But, such devices lead usually to very high pressure drops. Indeed, to address the problem of heat and mass transfer coefficients, high velocities of the fluid must be achieved, leading to high pressure losses and consequently to large mechanical power consumed by the pump. The flow distribution in the heat exchanger may be also difficult to control, potentially generating additional pressure losses.

Earlier studies to investigate the effect of corrugated channels were carried out numerically by Sunden and Trollheden [4]. These authors investigated laminar convective flow and heat transfer in a corrugated two-dimensional channel under constant heat flux conditions. Heat transfer coefficient was found to be increased when Prandtl number was high ($Pr = 5$) while the pressure drop was very significant.

Kanaris et al. [5] studied numerically the flow and heat transfer in a triangular corrugated channel. The corrugations were on the upper wall while the lower was flat. A constant temperature was imposed on the lower wall. Turbulence model (SST: Shear Stress Transport) was used to solve the heat transfer and flow equations for Reynolds number ranging from 400 to 1400. The authors found that the performance depends on the Reynolds number and is better than the one obtained with a smooth channel.

Naphon [6] conducted a numerical study on various corrugation geometries arranged in in-phase and out-phase layouts (e.g. flat plate, arc-shaped, trapezoidal and V-shaped) to enhance the thermal performance. He obtained that for a given air flow rate, V-shaped corrugated channel has the most significant effect on the enhancement of the heat transfer.

Zhang et al. [7] studied the impact of roughness in microchannels that were represented by triangular, rectangular and semicircular roughness elements, respectively. These authors found that these roughness elements contribute significantly to the heat transfer rate and to the pressure drop as compared to smooth channel. Thermo-hydraulic performances decrease considering successively semicircle, triangular and rectangular roughness elements. It was also revealed that the roughness elements induce stronger recirculation and flow separation when increasing the roughness height. These effects are dominant with semicircular and triangular roughness elements while they are weaker with rectangular roughness element.

Mohammed et al. [8] numerically investigated the fluid flow and heat transfer characteristics in a 2-D V-shape corrugated parallel channels in turbulent regime ($8000 < Re < 20000$). The effects of geometrical parameters such as the wavy angle, wavy height and channel height on the flow and thermal fields were examined. It has been found that pressure drop increased with the increase in the wavy height, and wavy angle while it decreased with the increase in the channel height. Similarly, heat transfer increased with the increase in the wavy channel and wavy angle while it decreased with the increase in the channel height.

So, miniaturization of thermal systems involves finding dedicated solutions to maintain acceptable pumping power of the fluid simultaneously with high heat transfer and mixing efficiency. Léal et al. [9] presented an excellent review focused on active heat transfer intensification methods. One possible way to simultaneously disturb the boundary layers and to integrate the pumping function within the heat exchanger is to generate a dynamic deformation of at least one of the channel's wall. Indeed, the disturbance of the boundary layer can be achieved by using progressive wave deformation of the wall (similarly to what is done in a peristaltic pump).

A few authors have conducted a series of experiments and numerical simulations to study unsteady fluid flow and heat transfer in corrugated channels. Nakamura et al. [10] investigated numerically the influence of the wall oscillation on the heat transfer characteristics in a two-dimensional channel. Comini et al. [11] studied the effect of space ratio (defined as channel height to length of a corrugation module) and corrugation angle on convection enhancement in unsteady state in wavy channels. These authors found that both the friction factor and the Nusselt number increase continuously when the corrugation angle increases (corresponding to more waves along the channel length) while they increase only up to a certain value when space ratio increases. Hossain and Islam [12] studied thermo-hydraulic properties in unsteady state in a sinusoidal wavy channel. They obtained a critical Reynolds number that depends on geometric configuration. It has been observed that flow becomes unsteady at lower Reynolds number while decreasing the channel height. They also found out that increasing the amplitude for a given channel height intensifies the instabilities and thus results in high heat transfer rate and pressure drop. However, impact of unsteadies was found to be almost insignificant on global results when changing by 20% the corrugation wavelength.

Kumar et al. [13] studied heat transfer inside circular millimeter size tubes with both static and moving sinusoidal corrugated walls. Numerical analyses were performed to study the effect of spatial wavelengths ($\lambda = 1/2, 2/3, 1, 2$ mm), Reynolds number (1–120) and amplitude (1–20% of tube diameter) on heat transfer and pressure drops. The heat transfer coefficient for the moving wavy walls (standing waves) had a higher value for all frequencies compared to the static wall case (up to 35–70%). A sharp decrease in pressure drop (by a factor of 1.2–5) was also obtained at high amplitudes. Mainly, heat transfer and pressure drop values apparently changed erratically with wall frequency. No general trends of heat transfer and pressure drop values with respect to operating parameters were found.

Léal et al. [14] presented a numerical study to determine both fluid flow and thermal performances when one of the channel walls of a heat exchanger was set in motion in a sinusoidal way. The considered virtual prototype was a dynamically deformed rectangular channel. The pressure difference between the ends of the channel was imposed, as well as the heat flux on one of the wall (static). The second wall was adiabatic and dynamically deformed to generate a travelling wave, similarly to what can be observed in peristaltic pumps. It was then demonstrated that the pumping function could be integrated in the heat exchanger allowing enhancing the heat transfer in a significant way. Moreover, as the flow rate and the heat transfer coefficient were found to be closely correlated to both the amplitude and the frequency of the travelling wave, it becomes possible to control independently the value of pressure drop and the value of the heat transfer coefficient. Thus, this technique involving a dynamic deformation of one of the channel wall may be considered for practical applications.

According to these studies, the dynamic deformation of a wall efficiently enhances the heat transfer. Additionally, if the amplitude of the deformation is high enough, a peristaltic pumping can be obtained. It therefore appears possible to realize an interesting multifunctional device using such a deformable system to enhance the heat transfer performance as well as eliminate the requirement of an external pump. Indeed, the configuration proposed by Léal et al. [14] was an academic one in the sense that both the geometry and the boundary conditions were idealized. For instance, it was considered that there were no boundary effects on the wave shape, while in practical applications the deformable wall has to be fixed on channel borders. It was also assumed that the pressure difference between the ends of the channel was very low (and constant in their study). Such an assumption involves that there is no

pressure drop in the rest of the loop whatever the flow rate is.

The aim of the present paper is to study the thermo-hydraulic performances of a mobile corrugated channel within a heat exchanger by taking into account realistic boundaries and geometry. The chosen application is the cooling of electronics devices in which the quality of heat exchange between wall and fluid as well as pumping effect are very critical. So, the chosen length of the active channel is 5 cm which is slightly higher than usual CPU (central processing unit) cover size. As previously indicated, more realistic connection between the deformed wall and the static one at the boundaries has to be taken into account, as this transition between fixed and mobile wall zone could impact the flow behavior. As the dynamic device should be connected to the static tubing, two zones have also been added, at the inlet and outlet of the actuated zone. This allows modelling the transition between actuated and static parts of the system and so providing realistic velocity profiles at the ends of the heat exchanger.

3-D numerical simulations were performed using commercial software StarCCM+ [15] based on finite volume method in transient laminar regime. Parametric studies were performed on both straight and dynamic corrugated channels, both from local and global points of view for various imposed pressure differences and deformation parameters. The pumping performances as well as the thermo-hydraulic behaviors were systematically investigated for a millimeter scale heat exchanger as described in the following section.

2. Virtual prototype of dynamic corrugated channel

In order to study fluid flow and heat transfer characteristics in small-scale heat exchanger, a virtual prototype based on a flat and straight channel and further transformed in a corrugated channel has been developed as presented in Fig. 1. Such a dynamically deformed corrugated channel allows us gaining a better understanding of heat transfer and pumping performances that are influenced by several operating parameters.

In the studied configuration, the lower wall was fixed and subjected to a constant and uniform heat flux over the imprint of heating zone length (length, L of 50 mm), facing the actuated zone on the upper wall. The upper wall (also called “membrane” in the following) was dynamically deformed to define five sinusoidal periods along this length. This upper wall and the sidewalls were kept adiabatic. The height (δ) of the channel, defined as the average distance between the two walls, was 1 mm while the width (W) of the channel was 50 mm. The upper wall deformation is progressively damped along inlet and outlet zones. In order to avoid numerical bias induced by reverse flow effect across boundaries, the lengths of inlet and outlet sections (reservoir zones) that were static in nature have been chosen sufficiently long (50 mm) to ensure a hydro-dynamically established flow at the entrance of the heated zone and to minimize boundary constraint at the exit of the actuated zone. Furthermore, a no-slip condition was imposed on all the physical walls.

In case of dynamic (moving) corrugated mini-channel, a mechanical power (W_P) was applied on the upper wall (see Fig. 1b). During the operation of dynamic corrugated mini-channel, W_P is dissipated into two forms: P_P (pumping power) and W_F (viscous dissipation) i.e. $W_P = W_F + P_P$. In the present study, the functioning of dynamic corrugated mini-channel was obtained by imposing different values of positive pressure differences ($\Delta P_s = P_{out} - P_{in} > 0$) between outlet and inlet of the exchanger. This pressure difference is used to mimic experimental conditions where the device is inserted between two fluid reservoirs at different altitudes (the upper reservoir being at the outlet). It then explains why a reverse flow can occur if pumping effect is not sufficient. In this latter case, an additional pump is required for the fluid to flow in the direct (or desired) direction as it could be with a conventional approach in classical heat exchangers.

This virtual prototype (see Fig. 1) intends to be representative of what could be a physical one. In the case of a physical prototype, the actuated wall has to be soft enough to be deformed with a reasonable force. It could be made with a thin metallic plate or a polymer membrane for instance. This membrane has to be fixed on its borders to ensure the sealing. Necessarily, a zone exists where the amplitude of the deformation evolves from the amplitude of the actuators to zero in the border zones. To take into account this constrain, damped deformation zones have been considered in the simulation, as described in the following (section 2.2). The force can be provided using, for instance, piezoelectric actuators, each of them being controlled by an electronic control unit.

To be really representative of a physical prototype, the main difficulty concerns the wave shape. Indeed, in a physical prototype, the number of actuators will be limited. It will then be difficult to obtain a perfect sinusoidal wave. Nevertheless, as the wave shape is intimately correlated with the number of actuators and the way they are fixed on the membrane, we chose to consider a sinusoidal wave shape in the present work.

3-D numerical simulations were carried out using the commercial software StarCCM+. This software allows modelling fluid flow and heat transfer in dynamically deformed structures. The flow was considered transient, three-dimensional and laminar. The working fluid was liquid water (at 27 °C) whose all thermo-physical properties were supposed constant for systematic studies. Moreover, impact of variations in thermo-physical properties was studied for some configurations. The imposed heat power (Γ) on the imprint (heated zone) was 125 W. Parametric studies were carried out for the cases where the wave amplitude varies from 60% up to 98% of the channel height (δ) with an imposed frequency of 50 Hz. The average height of the channel i.e. the mean height of the membrane (δ) is kept constant. The change in amplitude thus changes the extreme distance between membrane and heated wall. The results presented focuses on the “active zone” namely between S_1 and S_2 sections (see Fig. 1). All representative thermo-hydraulic quantities were calculated in this zone. The influence of relative amplitude (A) at various ΔP_s for a given frequency (f_r) and wavelength (λ) on thermo-hydraulic performances is studied.

2.1. Governing equations

The incompressible laminar and transient conjugate flow and heat transfer problems were solved considering that the dissipation source term is negligible and considering that the physical properties of the fluid are constant and uniform, using the classical combination of continuity, momentum and energy equations:

$$\vec{\nabla}\cdot\vec{u} = 0, \tag{1}$$

$$\rho\frac{\partial\vec{u}}{\partial t} + \rho(\vec{u}\cdot\vec{\nabla})\vec{u} = \rho\vec{g} - \vec{\nabla}\cdot\bar{\bar{P}} + \mu\Delta\vec{u}, \tag{2}$$

$$\rho C_p\left(\frac{\partial T}{\partial t} + \vec{u}\cdot\vec{\nabla}T\right) + \rho\vec{u}\cdot\frac{\partial\vec{u}}{\partial t} + \frac{\rho}{2}\left(\vec{\nabla}\left\|\vec{u}^2\right\|\right)\cdot\vec{u} = k_f\Delta T + \frac{\partial P}{\partial t}, \tag{3}$$

where, ρ is the density, $\vec{u}$ is the velocity vector, P is the pressure, T is the temperature, μ is the dynamic viscosity, C_p is the specific heat capacity, k_f is the thermal conductivity of fluid and $\vec{g}$ is the gravity acceleration.

The numerical resolution used a segregated approach with

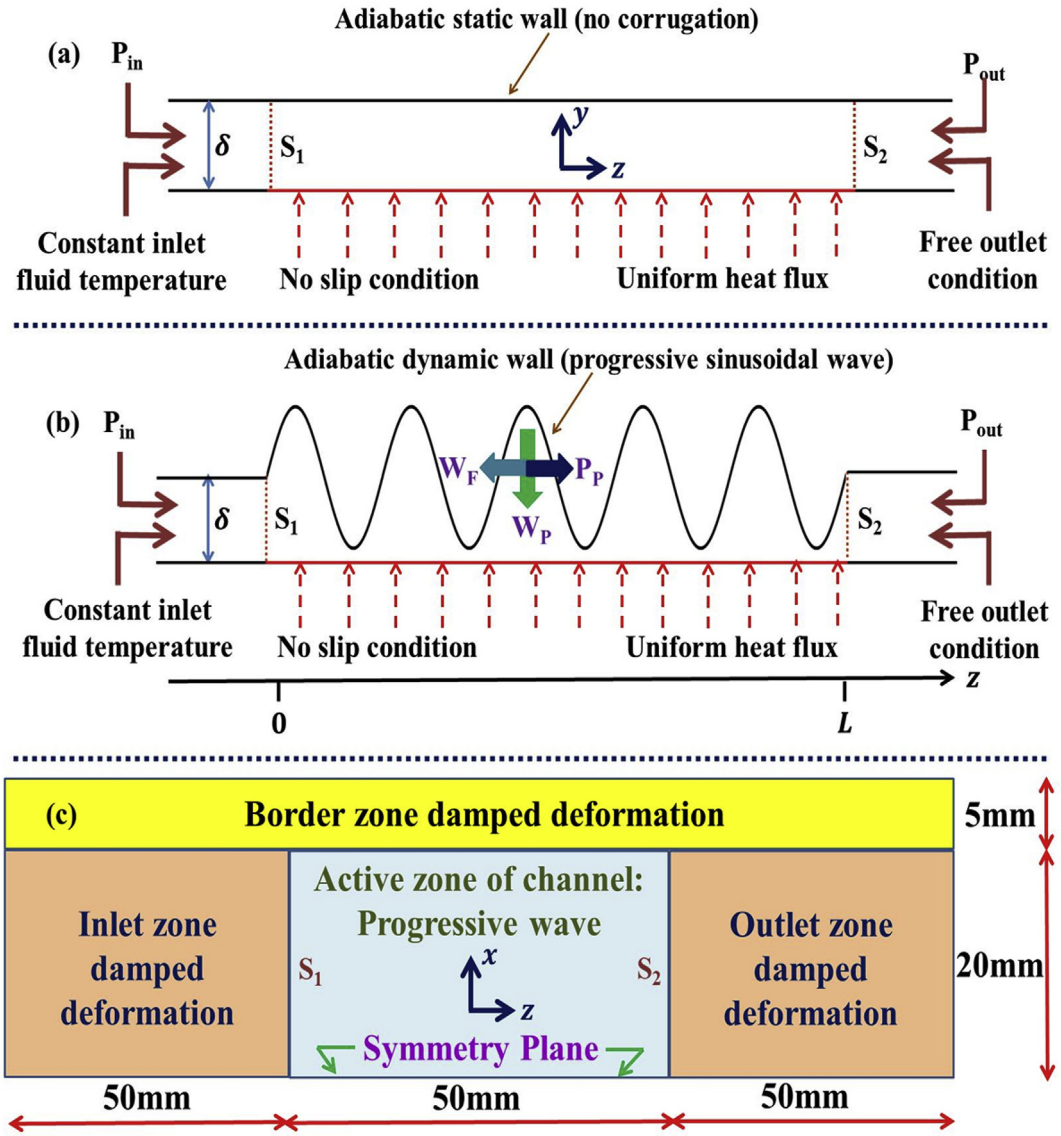

Fig. 1. The dynamic corrugated heat exchanger. 2-D schema of (a) flat channel where the upper wall is straight and static, (b) corrugated channel where the upper wall is dynamically deformed. The lower wall is uniformly heated. The upper wall (straight and deformed) was kept adiabatic. A positive pressure difference ($\Delta P_s = P_{out} - P_{in} > 0$) is imposed between outlet and inlet sections of the channel. (c) Top view of half of the channel model. The symmetry plane is the bottom line of this figure.

implicit second order temporal discretization and ad hoc relaxations factors in order to obtain adequate convergence behavior.

2.2. Management of dynamic corrugated wall

Three functions have been used to impose the displacement of the mobile wall of the channel. The first describes the progressive sinusoidal wave, while the other two functions damp the movement in the vicinity of the lateral walls, as well as at the inlet and outlet of the actuated zone.

In the proposed heat exchanger configuration, the average height of the channel is fixed while the minimum gap (distance between the lowest point of the membrane and the lower wall) varies as a function of the relative amplitude. The displacement of the upper wall (membrane) is defined by:

$$y(z,t) = \delta(1 + AY_1Y_2 sin(2\pi(f_r t + \omega z))), \quad (4)$$

where, δ is a constant displacement used to control the channel height, A is the relative amplitude of the displacement, Y_1 and Y_2 are two damping functions that take into account the different membrane effects in the vicinity of the boundaries of the actuated zone, f_r is the frequency, t is the time and ω is the number of waves per unit length, respectively.

A given point (not damped) on the moving wall stays in average at δ and move vertically from $\delta(1 - A)$ to $\delta(1 + A)$ and moreover, for static and straight channel, $A = 0$.

In order to take into account membrane fixation on the channel borders (only one clamped lateral border is shown on the virtual prototype due to the z-axis symmetry), two damping functions are defined in equations (5) and (6). These damping functions account for the deformation due to actuators in the border zones and take into account the realistic 3-D geometrical configuration of dynamic heat exchanger.

- For lateral damping, the amplitude is quickly reduced in order to obtain a realistic behavior corresponding to the transition

between a central zone where the membrane is fixed to an external moving device and the border where it is fixed (e.g. clamped) to close tightly the channel:

$$if\ \ x > 0.0015m : Y_1 = 1, \tag{5a}$$

$$else : Y_1 = \left(\frac{x}{0.0015}\right)^3. \tag{5b}$$

- For longitudinal damping, the sinusoidal wave is progressively damped in inlet and outlet zones. This was chosen to model a buffer zone where the "free" membrane oscillations decrease progressively thus inducing moderate stress on the material:

$$if\ \ z > 0.05m\ \ and\ \ if\ \ z < 0.10m : Y_2 = 1, \tag{6a}$$

$$if\ \ z > 0.10m : Y_2 = \left(1 - \frac{z - 0.10}{0.05}\right)^4, \tag{6b}$$

$$if\ \ z < 0.05m : Y_2 = \left(\frac{z}{0.05}\right)^4. \tag{6c}$$

2.3. 3-D numerical simulations and meshing strategy

In the studied configuration, the vertical plane passing through the central axis of the channel is a plane of symmetry, so only half of the channel was simulated (W/2 = 25 mm). The imposed power on the modeled half-imprint was thus 62.5 W to carry out numerical simulations (see Fig. 1c). This allows us to reduce the number of mesh cells to optimize computation time by dividing the simulated configuration by two compared to its actual size. Note that the fluid flow was considered in z-direction while the width and height of the channel were considered in x- and y-directions, respectively.

The creation of a convenient mesh in such highly anisotropic geometrical configuration subjected to large amplitude deformations (up to 98% of channel height) was rather tricky while keeping a computational time low enough to carry out parametric study without sacrificing precision or convergence of the dynamic transfer.

As a first step, the rectangular channel corresponding to the expected minimal height (actuated channel) was meshed. A structured anisotropic mesh was used as it allows us to fix the required size along the three spatial directions. This original mesh was highly anisotropic as the extension of the channel is extremely large compared to its height. The mesh was globally structured with refinement near the walls in order to capture boundary layers. Further, it was then dynamically deformed in order to follow the desired sinusoidal corrugated shape and movement of the upper wall. This procedure allowed us to conserve adequate quality of mesh shape during the whole calculations as it is only elongated along the height (thus reducing anisotropy of the cells). It also allows keeping a fine enough mesh in the constriction and managing a reasonable anisotropy of the cells.

The static inlet and outlet regions were meshed in a relatively coarse way to save calculations time as this would not induce bias on the thermo-hydraulic phenomena in active actuated/corrugated region. This latter was finely meshed with refinement in the vicinity of the lateral walls while larger mesh cells were used near the symmetry plane (see Fig. 2). "Morpher" capabilities of the commercial software StarCCM+ were used to manage the movement of the wall as well as the induced mesh deformations. The wall motion redistributes mesh vertices in response to the movement of control points. This way of mesh morphing allows generating an interpolation field of control points and their associated displacements throughout the region which can then be used to displace the actual vertices of the mesh. The displacement of the point within a single time-step specifies an associated distance vector of each control point. A corrugated channel obtained after applying progressive sinusoidal wave equation is presented in Fig. 2.

2.4. Data reduction

In case of dynamic corrugated channel, surface averaged and volume averaged thermo-hydraulic quantities on over operating configuration were calculated as follow.

The Reynolds number and hydraulic diameter are defined by:

$$Re = \frac{\rho \vec{u} D_h}{\mu}, D_h = \frac{1}{\lambda}\int_0^{\lambda} \frac{4S}{p} d\lambda, \tag{7}$$

where S is the flow fluid passage area along the heated zone and p is the perimeter of the passage section, respectively.

The local heat transfer coefficient is obtained by the spatial and temporal averaged fluid temperature and wall temperature on a wavelength ($\lambda = 1/\omega$) and on a period ($\tau = 1/f_r$):

$$\overline{T}_w(z) = \frac{1}{\tau W}\int_t^{t+\tau}\int_{x=0}^{x=W} T_w(x,z,t)dxdt, \tag{8}$$

$$\overline{T}_{mf}(z) = \frac{1}{\tau \delta W}\int_t^{t+\tau}\int_{y=0}^{y=y(z,t)}\int_{x=0}^{x=W} T_{mf}(x,y,\ z,t)dxdydt. \tag{9}$$

The local heat transfer coefficient and Nusselt number are then defined as:

$$h(z) = \frac{q(z)}{\left(\overline{T}_w(z) - \overline{T}_{mf}(z)\right)}, Nu(z) = \frac{h(z)D_h}{k_f}. \tag{10}$$

In the following, the global heat transfer coefficient and Nusselt number across the channel are then defined as:

$$\langle h \rangle = \frac{\Gamma}{S\left(\overline{T}_w - \overline{T}_{mf}\right)}, \langle Nu \rangle = \frac{hD_h}{k_f}, \tag{11}$$

where, $< >$ denotes volume and surface averages for both fluid and wall between sections S_1 and S_2.

2.5. Mesh convergence criteria

The corrugation shape and fluid flow were first initialized for all studied cases. The chosen time step must be small enough to obtain an accurate description of the wall movement and of the dynamics of all thermo-hydraulic quantities: typically 20 up to 30 time steps per period are needed (see Léal et al. [14]). In the present work, 50 time steps per period were used to allow a precise description of all quantities. Then, calculations were carried out until a periodic stationary regime is reached. This latter point was checked by comparing temporal evolutions of global heat transfer and flow characteristics. The calculations over a long time have been performed till an excellent estimation of the established conditions is obtained when the heat transfer coefficient varies by less than 1%. Consequently, an additional time period was added to extract all instantaneous and time averaged values of all physical quantities.

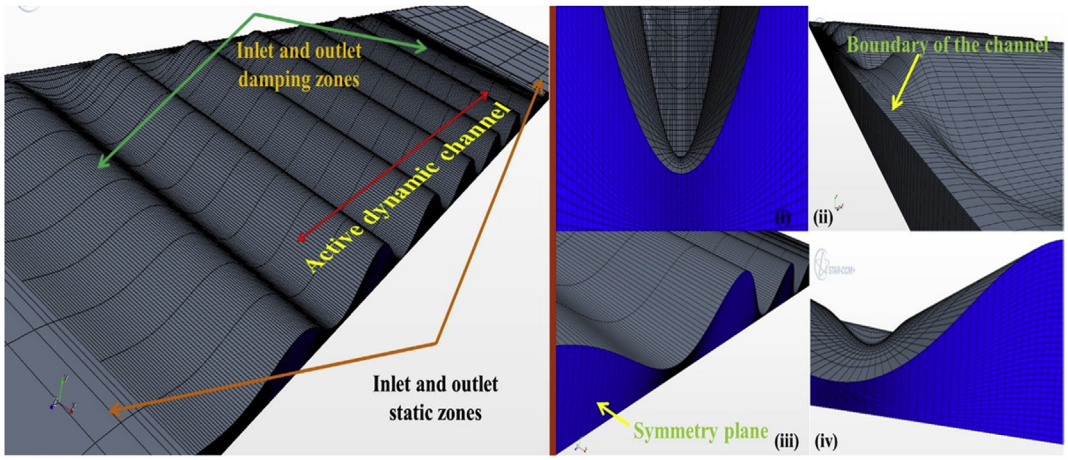

Fig. 2. The dynamic corrugated heat exchanger mesh. Left: Overview of mesh: static, damping and fully actuated zones of an overall dynamic sinusoidal corrugated channel. Right: Corrugated dynamic channel: (i) Zoom view of meshing at minimal channel opening at high deformation, (ii): Zoom view of fixed membrane at the boundary of the channel, and (iii and iv): Zoom view of fine meshing at crests and troughs at symmetry plane of the corrugated channel. The meshed images are presented for dynamic wall with $A = 95\%$.

The mesh convergence for a given time step per period is important to obtain representative results (see Table 1). In fact, if the mesh is too thin along height, the solver reaches the point where there is no residual convergence due to cells elongation and thus, no correct results can be obtained. Reducing significantly the cell size while keeping constant aspect ratio leads to unreasonable computational time. On the other hand, coarse meshing does not allow the solver to provide meaningful results.

From Table 1, it can be seen that the use of very small mesh size (corresponding to large number of cells) does not impact strongly on the global properties for different amplitudes indicating a fair convergence. Based on these observations and the percentage of variations in the global thermo-hydraulic properties, mesh sizes have been chosen corresponding to 281072 mesh cells to perform the systematic studies for dynamic corrugated channels.

3. Global thermo-hydraulic results

The global thermal properties, i.e. heat transfer coefficient with constant as well as variable thermo-physical properties of the fluid, were first compared in the case of the dynamic corrugated wall. Further, thermo-hydraulic characteristics of mass flow rate and heat transfer as function of the (positive) pressure difference between exit and entrance sections of the dynamic corrugated channel are presented in the following sections. In the present configuration, pressure difference was varied in order to study its impact on the performance of the system.

3.1. Comparison and validation with literature data

Numerical simulations were first performed on a flat rectangular channel (considering wave amplitude equal to 0). The results for pressure drops and velocity fields were found to be consistent with Poiseuille law in the fully developed laminar regime. The value of Nusselt number (Nu) in the fully developed flow was found to be 5.62 and compared with the experimental data of Lee et al. [16] who found $Nu = 5.4$. Note that these authors reported this value of Nusselt number for channel aspect ratio ≤ 0.1 while the aspect ratio of the present channel configuration is 0.02. This excellent agreement for the straight channel allowed us to explore the thermo-hydraulic performances of dynamic wall corrugated channel.

There are a very few data available in the literature for dynamic heat exchangers and thus, it is very difficult to compare the results of the present work. Léal et al. [14] performed numerical studies on such dynamic exchangers. However, there are a few differences in terms of corrugated channel configuration and operating parameters between their work [14] and present work. In their work, no damping zones were used (i.e. not a real 3D geometry), negative pressure difference between the outlet and inlet sections was imposed i.e. ΔP_s =-20Pa, the channel width was 30 mm and the number of sinusoidal waves used was 10. In the present configuration, two damping zones are used (allowing the membrane to seal with the borders), positive pressure difference is imposed, the channel width is 50 mm and 5 sine waves along the actuated zone are used. Note that the number of waves per meter is identical in both studies.

To be consistent with the works of Léal et al. [14], one set of numerical simulations on dynamic channel were carried out to compute the mass flow rate and heat transfer coefficient for $f_r =$ 50 Hz and ΔP_s =-20Pa. The obtained results using these boundary conditions were compared with the results reported in work of Léal et al. [14] for various relative amplitudes (see Fig. 3).

It can be seen in Fig. 3 that the simulated values of heat transfer coefficient are similar while mass flux is consistently higher (by a factor of 1.18) as compared to the data of Léal et al. [14]. Current numerical results are found to follow qualitatively the same trend. The distinction between the results can be attributed to differences in the channel configurations, in particular to the effect of the damping of the membrane in the border regions which was considered in the present work and not in the work of Léal et al. [14]. The comparisons and qualitative trend lend confidence to the current thermo-hydraulic results.

3.2. Impact of temperature dependent fluid properties

Impact of thermo-dependent properties of water (Faghri et al. [17]) on mass flow rate and heat transfer coefficient has been studied for an imposed positive pressure difference of $\Delta P_s = 50$Pa, as presented in Fig. 4. The variation in mass flow rate (ρQ_v) is about 1.5% in the studied range of the relative amplitude (A) which clearly suggests that the temperature dependence of the fluid properties does not significantly influence the mass flow rate for the moderate temperature variations obtained in such systems. Moreover, it can be observed that the heat transfer coefficient slightly increases for $A <$ 90% (variation in $h \approx$ 1%) or decreases for $A >$ 90% (variation in

Table 1
Mesh convergence. Global flow and heat transfer properties in dynamic corrugated channel case for different number of mesh cells for different imposed positive pressure differences ΔP_s (grey color case chosen to carry out systematic studies).

Positive pressure difference, ΔP_s (Pa)	Amplitude	Number of cells	Mass flow rate (kg/s)	Heat transfer coefficient ($W.m^{-2}.K^{-1}$)
50	60%	43560	9.570E-03	4988
		159766	1.317E-02	4957
		281072	1.277E-02	4921
	80%	43560	1.693E-02	6174
		159766	2.053E-02	6136
		281072	2.01E-02	6091
	95%	43560	–	–
		159766	2.621E-02	11561
		281072	2.58E-02	11477
500	60%	43560	2.320E-03	4149
		159766	5.920E-03	4123
		281072	5.52E-03	4093
	80%	43560	1.546E-02	5877
		159766	1.906E-02	5841
		281072	1.87E-02	5798
	95%	43560	–	–
		159766	2.579E-02	11340
		281072	2.54E-02	11257
1000	60%	43560	2.350E-03	5998
		159766	5.950E-03	5962
		281072	5.55E-03	5918
	80%	43560	1.406E-02	5723
		159766	1.766E-02	5688
		281072	1.73E-02	5646
	95%	43560	–	–
		159766	2.543E-02	11337
		281072	2.50E-02	11254

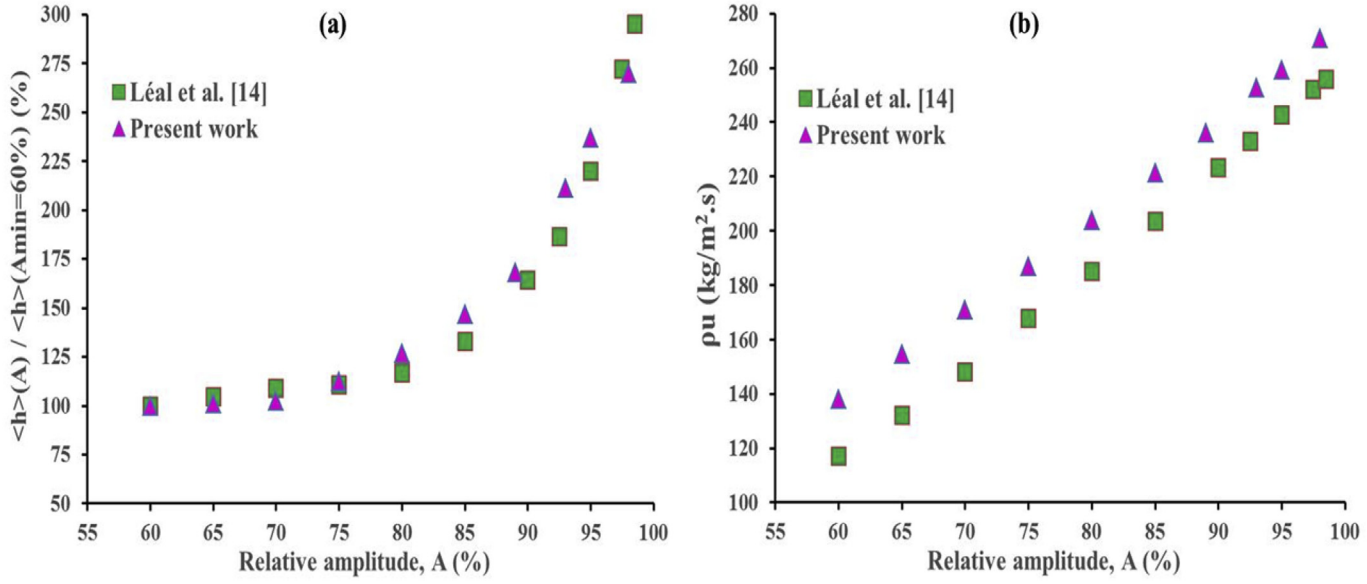

Fig. 3. Qualitative comparison of (a) heat transfer coefficient, and, (b) mass flux (ρu). Note that, the presented results are obtained for ΔP_s =-20Pa and f_r = 50 Hz for both studies.

$h <$ 3%) compared to values obtained using constant properties of fluid.

In the considered amplitude range, 60% $< A <$ 90%, globally, the temperature difference between wall and water is slightly smaller compared to constant properties case while for very high amplitude ($A >$ 90%) this difference becomes higher because a temperature gradient starts to establish in the core of the moving corrugations. This behavior is mainly due to the fact that the flow structure is strongly driven by the wall movement and thus local viscosity variation only produces a minor change. Moreover, the wall displacement completely changes the thermal field compared to static case and disrupt boundary layers leading to a fairly homogeneous temperature in the fluid, thus limiting the properties variation effects.

As the global thermo-hydraulic properties were not influenced so much by the temperature dependence of the physical properties of the fluid, systematic studies were further carried out using constant fluid properties.

3.3. Local analysis

Local analysis is presented for the dynamic heat exchanger with A = 89% and ΔP_s = 10000 Pa at various times in Fig. 5. During expansion of the dynamic channel, the fluid moves in the

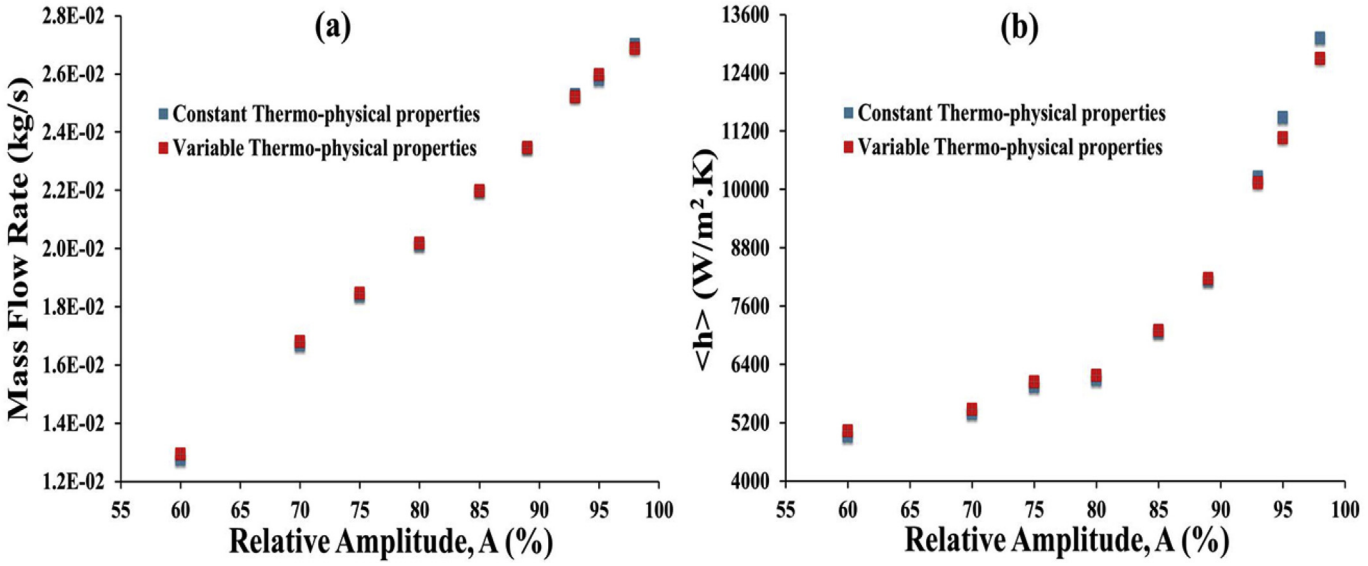

Fig. 4. Impact of thermo-dependent fluid properties. Global (a) mass flow rate (ρQ_v) and (b) heat transfer coefficient (h) obtained using constant and variable thermo-physical properties as a function of the relative amplitude for dynamic corrugated channel when $\Delta P_s = 50$Pa and $f_r = 50$ Hz.

longitudinal direction because of the progressive wave. Wall movement induces vertical (i.e. towards heated wall) displacement of the fluid. Due to progressive movement of the channel wall, cold fluid is moved near the heated wall at every location; this boundary layer disruption increases sharply heat transfer along with mixing that takes place within the core flow.

There is an increase of the pressure according to z-direction in the actuated zone that can be observed as stair like profile contrary to what is observed in classical flat and straight channel. This phenomenon leads the fluid flowing in the hydraulic circuit and thus eliminating requirement of an external pump. Such a longitudinal increase of the pressure in the actuated region helps in increasing the mass flow rate, which in turn results in high heat transfer.

3.4. Impact of pressure difference ($\Delta \boldsymbol{P_s} > 0$)

In the studied configuration, pressure differences($\Delta P_s = P_{out} - P_{in} > 0$) have been applied between outlet and inlet sections of the channel. This mimics the situation where the device is placed between two reservoirs located at different altitudes and the aim is to transfer the fluid from the low level reservoir (inlet) to the high level reservoir (outlet). In this case, the fluid flows towards high pressure side due to the pumping action induced by the dynamic wall contrary to conventional heat exchangers (see Fig. 6).

Thus, the proposed heat exchanger generates the pressure gain to eliminate the need of external pump. The movement of dynamic wall, amplitudes and pressure differences are coupled with heat transfer coefficient and mass flow rate. A separate analysis of thermal-hydraulic characteristics in terms of mass flow and heat transfer coefficient is presented in the following sections.

3.4.1. Systematic analysis

The systematic studies of mass flow rate and heat transfer coefficient for imposed pressure difference are detailed in the following sections.

3.4.1.1. Mass flow rate. As expected, the mass flow rate depends primarily on the amplitude of deformation imposed on the mobile wall. Increasing amplitude thus leads to a proportional increase of the mass flow rate (see Fig. 7a). However, the mass flow rate decreases with the increase of the pressure difference at given amplitude (see Fig. 7b). Again, this behavior was expected. Indeed, the pressure difference between outlet and inlet of the exchanger is positive, corresponding to pressure gain that is induced by the mechanical power from membrane actuation. A slight decrease in flow rate (about 25%) was observed for the higher pressure difference while the prescribed outlet-inlet pressure differences were varied over several orders of magnitude. The system behaves therefore, from a hydraulic point of view, as a quasi-volumetric pump if amplitude is high enough. Indeed, at low amplitude the actuated zone is limited to a small fraction of the channel section and the fluid may flow in reverse direction in the lower part of the channel (i.e. part of the channel far from the sine waves and close to the static lower wall). The variations of mass flow rate with pressure differences are of course more pronounced for small amplitude wave, while for a complete occlusion of channel (A= 100%), a perfect volumetric pump behavior would be observed.

3.4.1.2. Heat transfer coefficient. The heat transfer coefficient also depends on the amplitude for a given average channel height. The higher the amplitude, the more significant is the heat transfer intensification compared to cases without deformation/corrugation (straight channel) as presented in Fig. 8a. This behavior can be explained by the following considerations:

- Majority of the heat transfer occurs where the thermal resistances are the lowest, i.e. at the strongest constrictions in the channel. These constrictions are located where the cross section for the flow is lowest (see Fig. 9a). In this figure, the temperature field close to the lower wall shows that at these constrictions, the fluid temperature is significantly lower leading to the enhancement in heat transfer rate. The value of the heat transfer coefficient is thus no longer controlled by the average size of the channel, but by the smallest dimension, leading to very high values of the heat transfer coefficient.
- The dynamic corrugation of the upper wall of the heat exchanger causes a mixing intensification (see Fig. 9a). In fact, the upper wall pushes the fluid at the constrictions and then

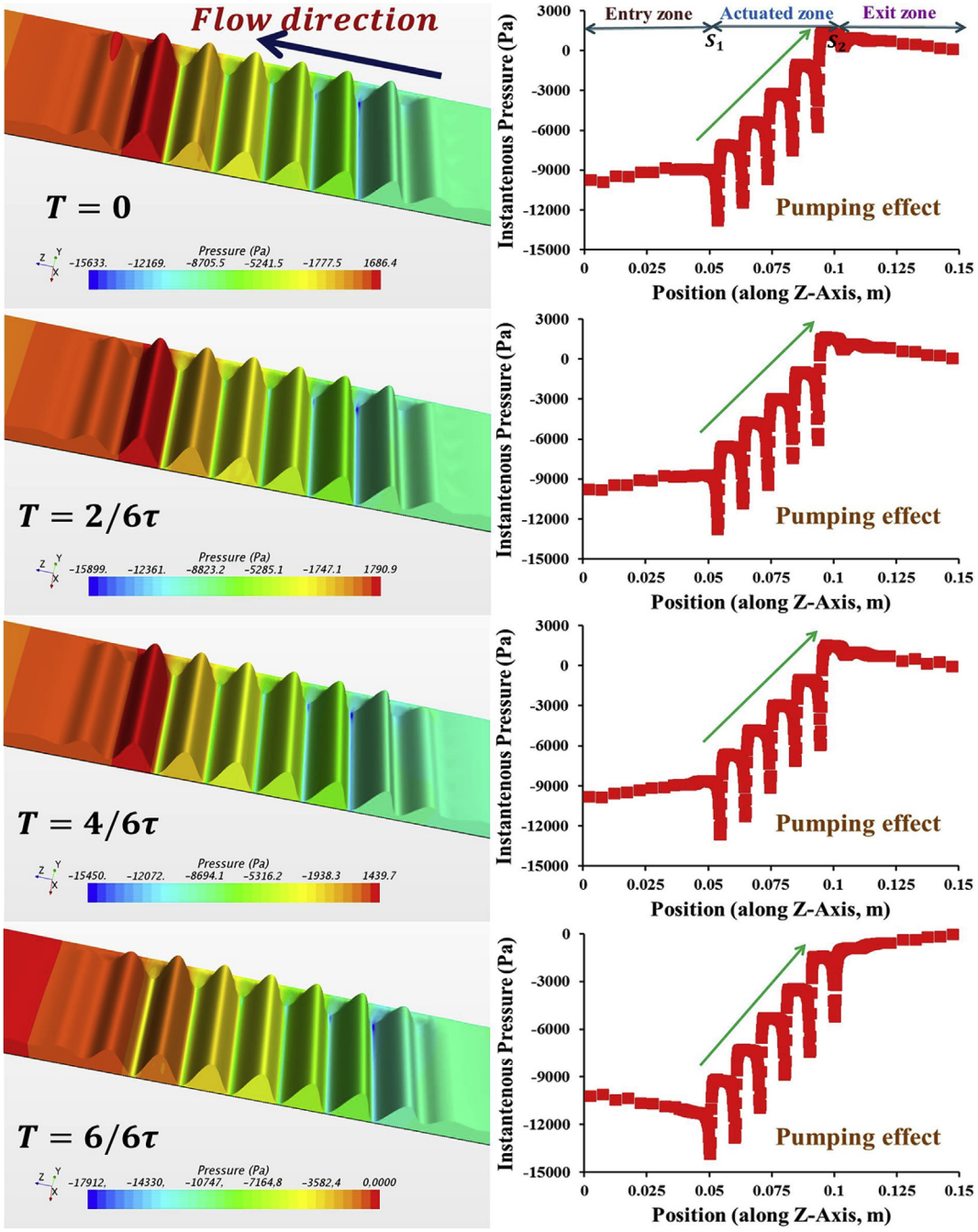

Fig. 5. Local analysis. Left: Instantaneous pressure field; Right: Pressure profile along the channel length in the dynamic heat exchanger corresponding to instantaneous time. Stair like profile in actuated zone: Pressure increases in each sinusoidal pocket. Results are presented for $A = 89\%$, $\Delta P_s = 10000$Pa and $f_r = 50$ Hz.

two phenomena appear that contribute to the mixing effect. The first phenomenon can be described by a local jet which is flowing in the global reverse flow direction. This is due to the combined effect of the dynamic wall and the imposed pressure difference between the outlet and the inlet (see Fig. 9b and c). Note that, this local jet is stuck to the dynamic wall, which is one of the major contributions in developing the mixing effect. The second phenomenon can be described by the stationary fluid in the wave pocket which is pushed in the global desired flow direction. Thus, it flows in the opposite direction of the local jet and the combination of these two phenomena forms a vortex-like process in the pocket. Therefore, this mixing intensification causes a disturbance in the establishment of the thermal boundary layer by bringing colder fluid close to the heated wall and thus, leading to the intensification in the heat transfer.

At very high amplitude, the heat transfer coefficient vary neither as a function of pressure difference nor as a function of the mass flow rate as shown in Fig. 8b. In fact, for high amplitude and moderate pressure difference, the system acts as a volumetric pump and compensates its own viscous losses. The mass flow rate and consequently the heat transfer coefficient are then relatively independent from the pressure difference.

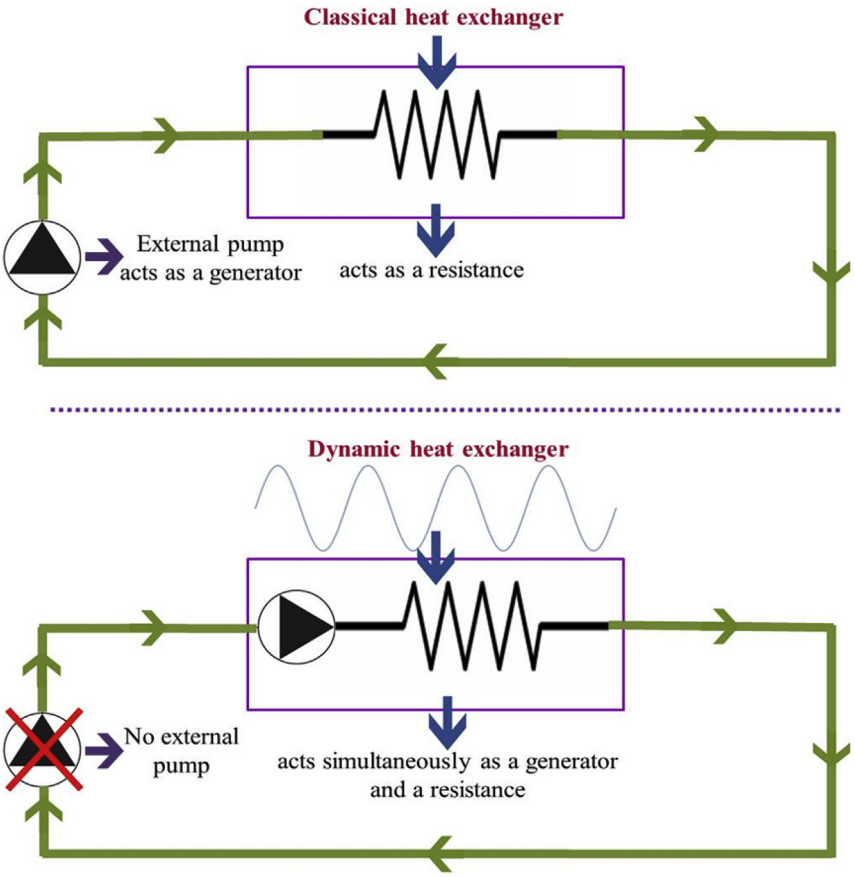

Fig. 6. Classical versus new dynamic heat exchanger. Schema of a heat exchanger with an external pump (top) and without external pump (bottom) by integrating dynamic wall in the heat exchanger.

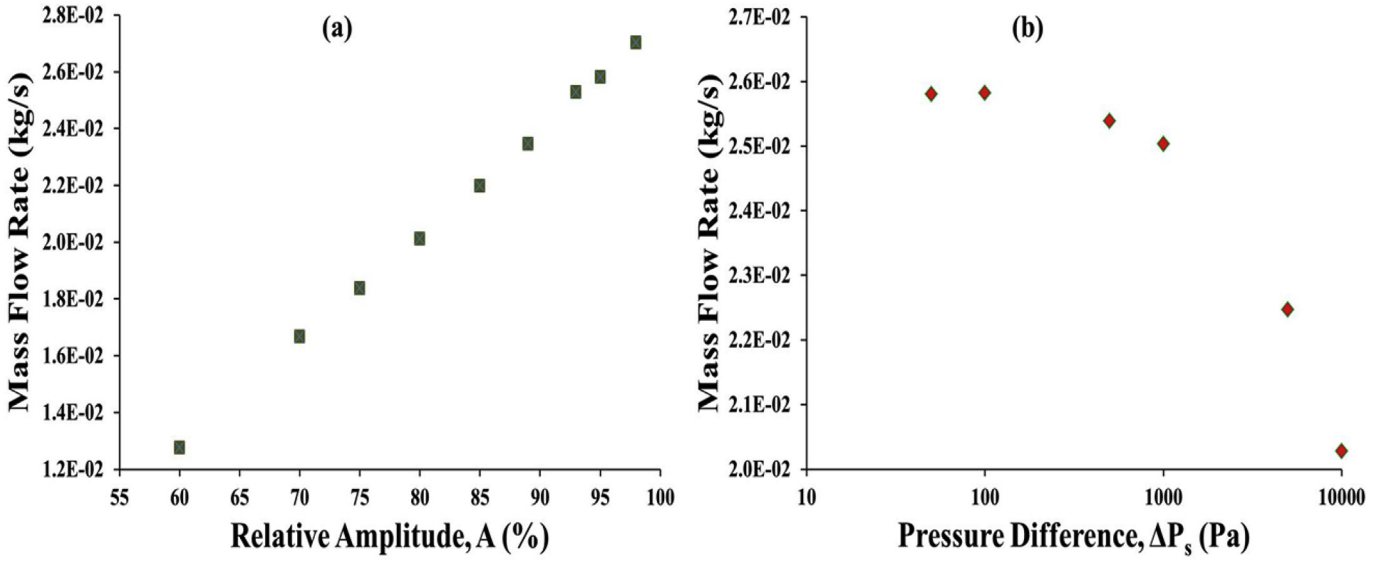

Fig. 7. Systematic analysis on mass flow rate. (a) Mass flow rate as a function of relative amplitude when $\Delta P_s = 50$Pa, (b) Variation in mass flow rate with imposed pressure difference for $A = 95\%$. $f_r = 50$ Hz.

3.4.2. Global analysis

The use of dynamic wall at high amplitudes (A> 90%) allows obtaining significant heat transfer coefficient for any imposed pressure difference (see Fig. 10a). No influence of this pressure difference is found on heat transfer in that case. On the other hand, it can be observed that the variations in heat transfer coefficient at lower amplitudes are more difficult to predict when the pressure difference between the ends of the exchanger increases; the evolution of the heat transfer coefficient is no longer monotonous. However, when the amplitude is low, a high pressure difference

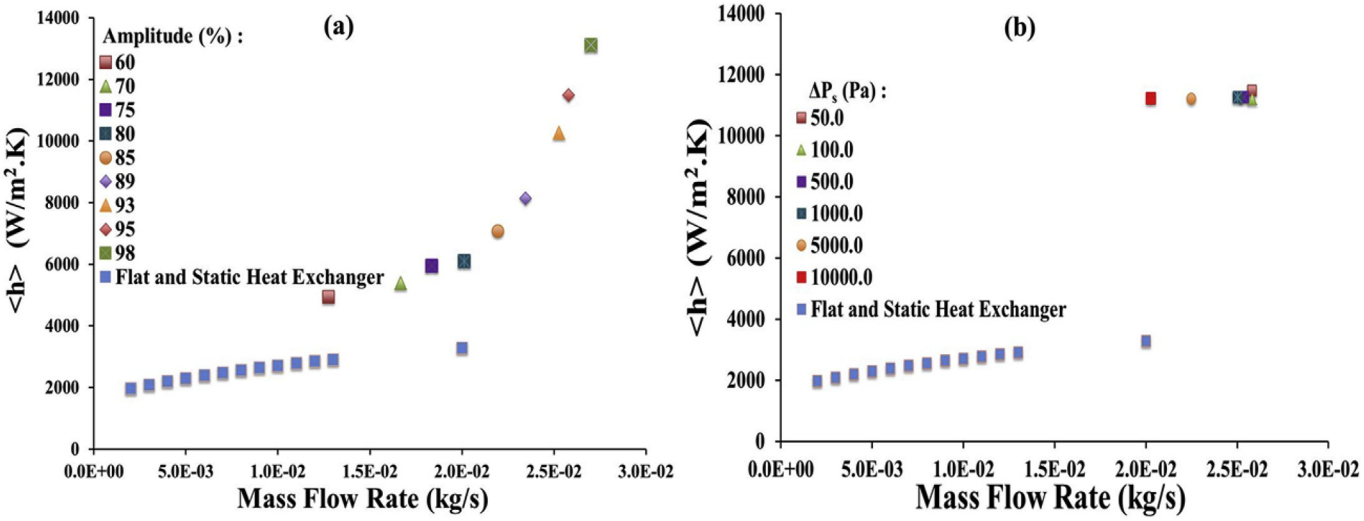

Fig. 8. Systematic analysis on heat transfer coefficient. Global heat transfer coefficient (h) as a function of mass flow rate for (a) different relative amplitudes and a $\Delta P_s = 50$ Pa, and for (b) different ΔP_s for a relative amplitude of 95% for the dynamic corrugated channel. $f_r = 50$ Hz. Comparison with flat and static channel is also presented.

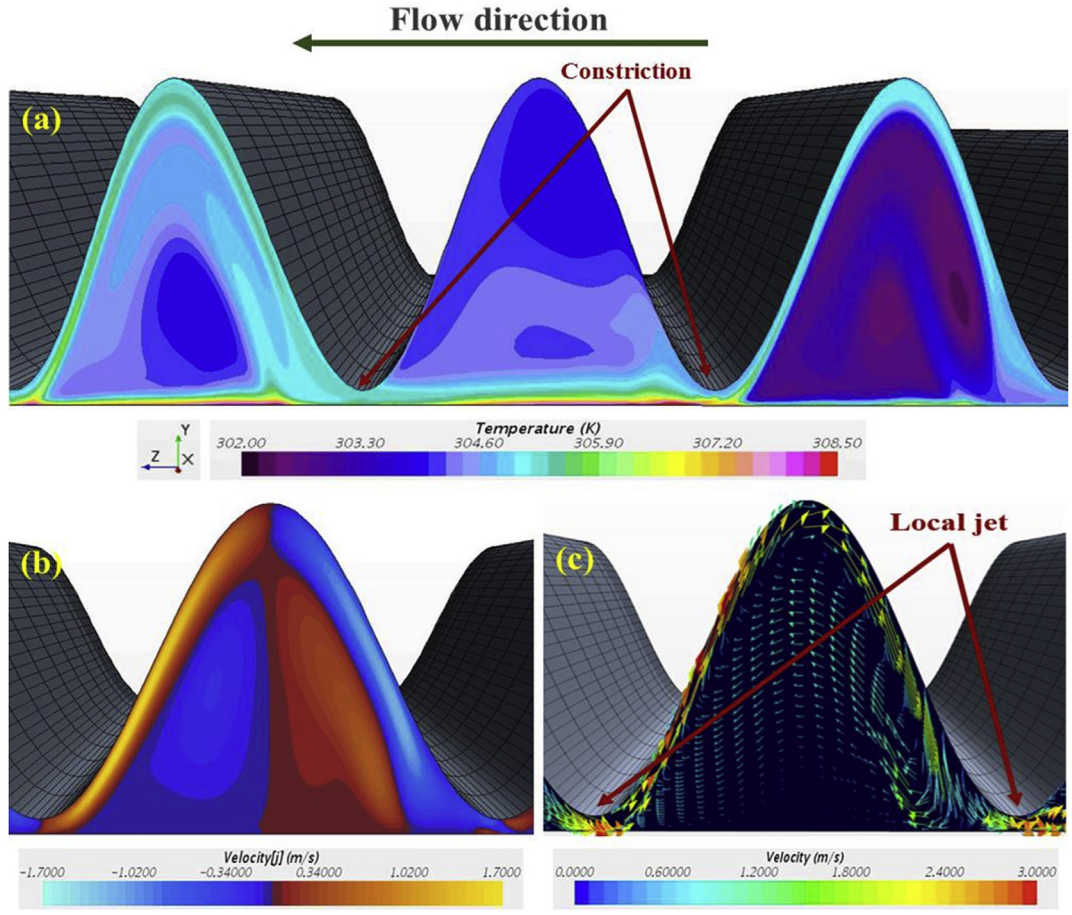

Fig. 9. Magnified views of the dynamic corrugated heat exchanger at the symmetry section. (a) Temperature field, (b) Vertical velocity field, and (c) Velocity vectors field are shown. The images are presented at a given instantaneous time for $A = 85\%$, $f_r = 50$ Hz and $\Delta P_s = 500$Pa.

($\Delta P_s = 5000$ and 10000 Pa) leads to a high value of the heat transfer coefficient compared to the case of small values of pressure difference. This is particularly visible for amplitude of 75% and $\Delta P_s =$ 10000 Pa. Indeed, the mass flow rate under the same conditions (A= 75% and at $\Delta P_s = 10000$ Pa) is close to 0 kg/s, involving that the fluid moves back and forth in the exchanger due to high exit pressure. Similarly, mass flow rate depends on amplitude as well as on imposed pressure difference (see Fig. 10b). It is observed that, for high pressures at the exit, the fluid goes in the opposite direction to that of the desired direction (negative mass flow rate) at low

amplitudes but remains well controlled for the high amplitudes. There are significant variations in mass flow rate (negative and positive) at high values of the pressure difference and low amplitudes, while at high amplitudes; change in pressure difference does not impact strongly the mass flow rate.

It strongly reflects the fact that the proposed dynamic corrugated channel within the exchanger does not have to be coupled with external pump for the fluid flow when pressure at the outlet is more important than the inlet. Moreover, it seems to perform very well to generate the fluid flow by its own virtue and have high heat transfer coefficient.

4. Merit factor

In the studied configuration of dynamically deformed heat exchanger within mini-channel, the determination of its performance is not straightforward. It is therefore, interesting to compare the performance of the proposed dynamic heat exchanger with a static corrugated heat exchanger. In this case, the pressure drop of such system must be obtained in terms of pressure dissipations of the system.

The pressure drops come from the viscosity effects and thus are called viscous dissipations, W_F. These losses ($W_F = W_P - P_P$) in the actuated system can be calculated by obtaining the mechanical power applied on the actuated surface (W_P) and the pumping power produced by the system (P_P).

Since there is no work of the tangential forces on the dynamic wall, the mechanical power can be simply computed by integrating the pressure stress on the entire dynamic surface (static part obviously does not produce any work) and it is expressed as:

$$W_P = \int_{S_{dw}} \left(- P\bar{\bar{I}} \cdot \vec{n} \right) \cdot \vec{u} \; ds, \tag{12}$$

where, $P\bar{\bar{I}}$ is the pressure stress, S_{dw} is the surface of the dynamic wall and $\vec{n}$ is the normal vector to this surface.

The pressure gain (ΔP_g) in the actuated zone (between sections S_1 and S_2) leads in obtaining either pumping gain or loss, depending on the external conditions in dynamic heat exchanger. Thus, the pumping power (P_P) is computed through the simple formula below:

$$P_P = Q_v \Delta P_g, \tag{13}$$

where Q_v is the volume flow rate and $\Delta P_g = P_2 - P_1$. (P_2 and P_1 are the pressure values obtained at S_2 and S_1 sections respectively)

A dynamic heat exchanger may or may not have pumping effect. This is directly linked to the wave amplitude and imposed pressure difference (see also Fig. 10b). When there is a pumping effect, an external pump is not required i.e. direct flow occurs between inlet and outlet of the exchanger. On the other hand, when there is no sufficient pumping effect, the heat exchanger remains the classical one i.e. reverse flow occurs between inlet and outlet of the exchanger and thus, an external pump is required. Note that, the heat transfer coefficient is always superior in both cases compared to static case (see discussion below and Fig. 12c). The occurrence of these phenomena is graphically presented using a flowchart in Fig. 11.

Viscous dissipation occurs in any heat exchanger device whether it is self-pumping or not. To evaluate the performance of a heat exchanger (static or dynamic), viscous dissipation (W_F) is required. In case of dynamic heat exchanger, viscous dissipation in the actuated zone is not relatively straightforward to calculate compared to classical one (static case) where pressure drop can be easily determined.

In the proposed configuration, the total mechanical power applied to the actuators is split into two effects. Globally, it can be transmitted into pumping power and viscous dissipation (see Fig. 1b). From the viscous dissipation, pressure drop in the actuated zone (between sections S_1 and S_2) of dynamic heat exchanger can be easily calculated.

The viscous dissipation (W_F) in the actuated zone of the dynamic heat exchanger is deduced using the following expression:

$$W_F = W_P - P_P, \tag{14a}$$

$$W_F = \int_{S_{dw}} \left(- P\bar{\bar{I}} \cdot \vec{n} \right) \cdot \vec{u} \; ds - Q_v \Delta P_g. \tag{14b}$$

For given amplitude (data presented for an amplitude of 89%), it can be observed that the mechanical power (W_P), the pumping power (P_p) and the viscous dissipation (W_F) increase with increasing imposed pressure differences (see Fig. 12a and Table 2).

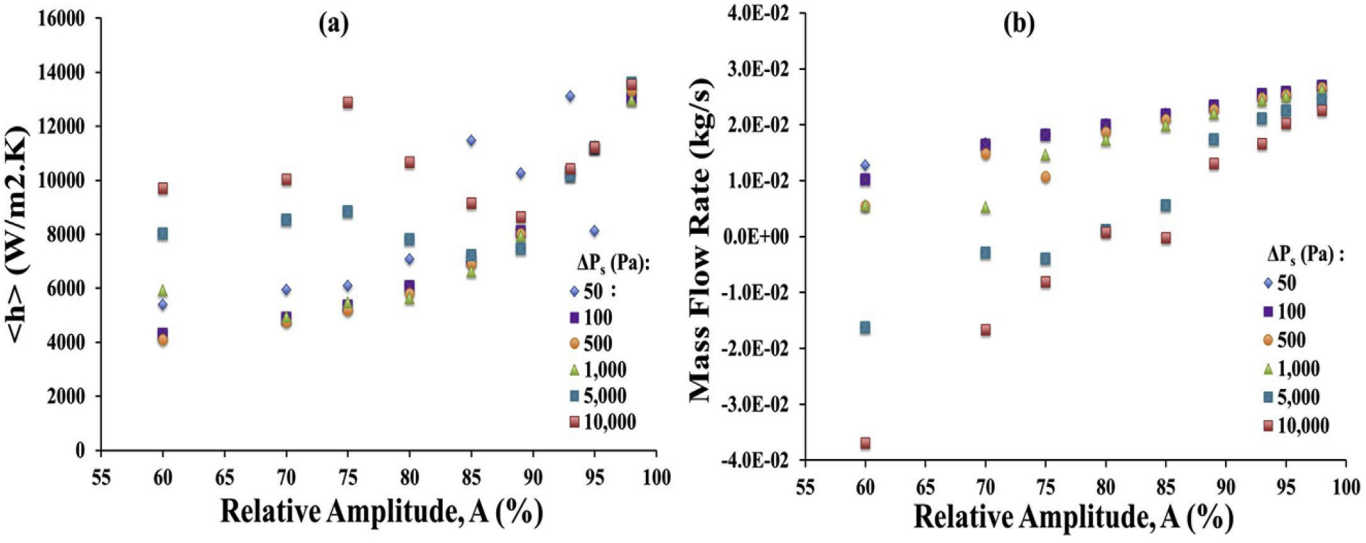

Fig. 10. (a) Global heat transfer coefficient (h), and (b) Mass flow rate, as a function of relative amplitude for different $\Delta P_s > 0$ and $f_r = 50$ Hz.

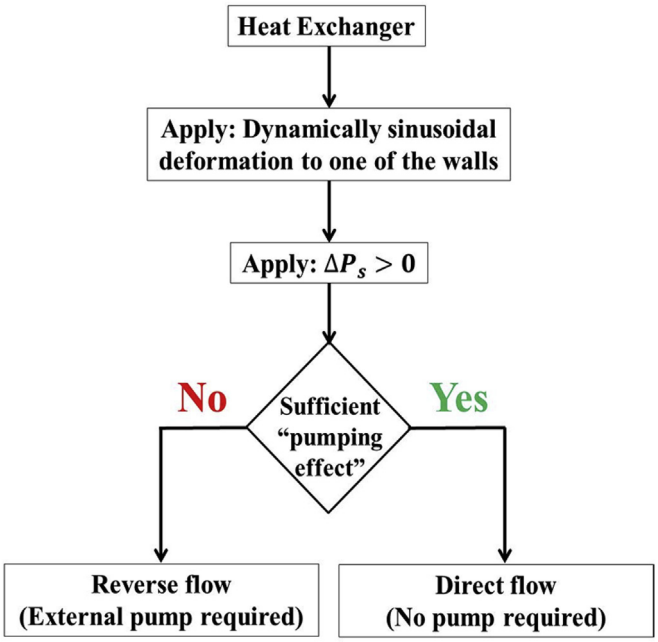

Fig. 11. Flowchart representation to describe direct and reverse flows in dynamic heat exchanger.

In fact, increasing the imposed pressure difference can be translated as increasing the flow resistance in the external system. Thus, the work on the dynamic corrugated wall has to increase to oppose this resistance, and subsequently, leading to increase in the pumping power and the viscous dissipation in return.

From the viscous dissipation (W_F), the equivalent pressure drop (ΔP_d) inside the actuated zone of the dynamic exchanger has been obtained using the following expression:

$$\Delta P_d = W_F / Q_v. \tag{15}$$

The higher the imposed pressure difference is, the higher is the pressure drop in the system (see Fig. 12a and Table 2). The higher value of external pressure drop limits the pumping effect of the system and thus, higher pumping power has to be generated by the system for the fluid to flow in the wave direction. Moreover, higher external pressure drop reduces the mass flow rate in the system. A simple explanation is that for low pressure difference, the fluid globally moves with the wave and circulating mainly where the section is maximal; the fluid velocity being very low in constricted zones. Thus, the velocity gradient and consequently, viscous dissipations are small. On the other hand, when the pressure difference is high, it leads the fluid to attempt to backflow with a high velocity below the constricted zone (depending on the amplitude) and thus, the velocity gradient and viscous dissipation increase leading to decrease the efficiency of the device. In order to get an optimal behavior, the amplitude has to be chosen according to the expected pressure difference in such a way that it ensures a direct flow through the device. Globally, it means that amplitude has to increase with pressure difference in order to keep the efficiency to a high value.

The easiest way to compare heat transfer rate and mass flow rate of static and dynamic corrugated channels (having the same geometrical configuration) can be performed at constant values of equivalent pressure drop (for a given amplitude). To do this, equivalent pressure drop obtained from dynamic channel (see Table 2) is applied on the static corrugated channel with and without lateral damping ($Y_1 = 0$ in case of no lateral damping). For the amplitude of 89%, heat transfer coefficients and mass flow rates were calculated for static corrugated channels and compared with the proposed dynamic channel (see Table 3). Note that, static corrugated wall without any lateral damping is the real 1-D case. To not forget that in the case of static channels, there is no self-pumping, contrary of the dynamic corrugated one. A comparative analysis of mass flow rates and heat transfer coefficients of different heat exchangers (static and dynamic) is presented in Fig. 12 (b and c) as a function of imposed pressure differences for different equivalent pressure drops.

Mass flow rate and heat transfer increase with increase in pressure drop in classical static corrugated heat exchangers as expected (see Fig. 12b and c). On the other hand, in case of dynamic corrugated exchanger, the behavior of mass flow rate is exactly opposite where it decreases slightly with increase in pressure drop and could attain the same value at very high pressure drops as in static corrugated case (see Fig. 12b). However, the values of mass flow rate in dynamic heat exchanger are always higher than static wall case (up to a factor of 37) between 50Pa and 1000Pa and then, it starts to decrease dramatically reaching almost the same value at very high pressure difference ($\approx$ 10000Pa). Heat transfer coefficient doesn't vary significantly as a function of pressure drop (or imposed pressure difference) in case of dynamic wall. Compared to static corrugated channel case, our proposed dynamic exchanger assists in very high heat transfer (up to a factor of 3–4) for a pressure drop less than 1000Pa while heat transfer coefficient tends to attain almost same values as of static corrugated case (see Fig. 12c) at very high pressure drop ($\approx$ 10000Pa). In fact, for static corrugated exchangers, the heat transfer coefficient increases with pressure drop as the flow is moving faster and it is then increasing the mixing and brings low temperature fluid close to the wall.

A comprehensive analysis of overall performance of the proposed heat exchanger has been performed and also compared with that of static corrugated channel. Many researchers use of the Colburn factor (j) to characterize heat transfer, rather than the Nusselt number (Nu) with friction factor (f). A surface having a higher j/f factor is "good" because it requires lower free flow area and hence a lower frontal area for heat exchanger (Kuppan [18]). The performance of heat exchangers can be evaluated as follows:

$$\frac{j}{f} = \frac{\frac{Nu}{RePr^{1/3}}}{\frac{\frac{\Delta P_d}{L} D_h}{\frac{1}{2}\rho \overrightarrow{u}^2}}, \tag{16}$$

where, ΔP_d is absolute value of pressure drop ($\Delta P_d < 0$).

Merit factors (j/f) of dynamic and static (with and without lateral damping) heat exchangers have also been evaluated for given amplitude of 89% and are presented in Fig. 12d (see also Tables 2 and 3). For each configuration (static and dynamic), friction factor is calculated from equivalent pressure drop and velocity (obtained from mass flow rate) while Nusselt number is calculated from the heat transfer coefficient (see Tables 2 and 3). Due to almost invariant values of heat transfer coefficients and decreasing trend of mass flow rate at different pressure drops, the performance of dynamic heat exchanger decreases with increasing pressure drop. On the other hand, increase in merit factor is obtained as expected in case of classical static corrugated channel as a function of pressure drop. It can be noticed that the proposed heat exchanger performs greatly and has higher overall performance (j/f) by a factor of 35–115 compared to static corrugated channels for the pressure drops below 1000Pa. Contrary to this effect, the overall performance of dynamic exchanger starts to decrease significantly with increasing pressure drop. Further, it reaches the same performance than static corrugated case.

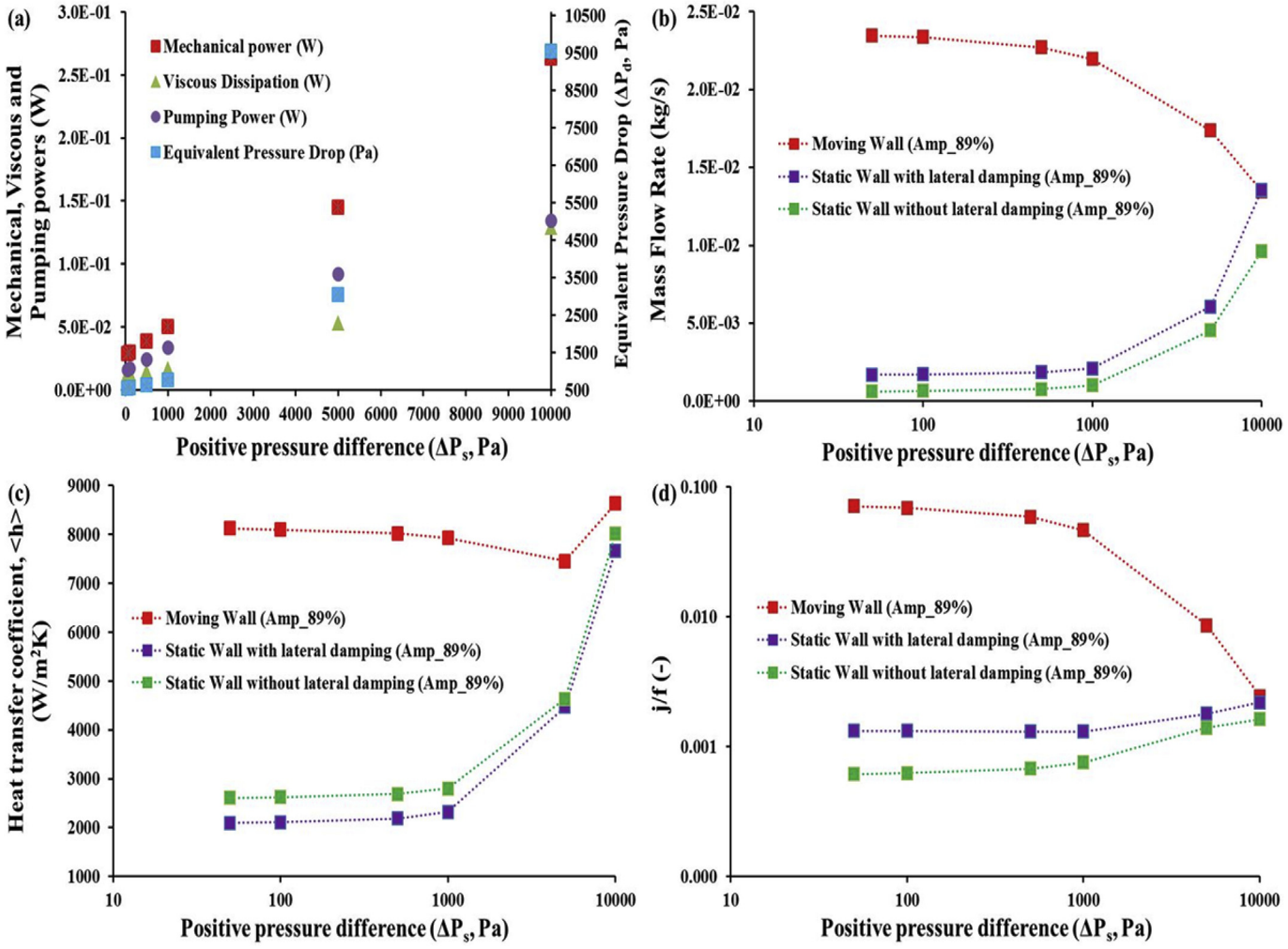

Fig. 12. Performances of the dynamic corrugated heat exchanger. Presentation of (a) the mechanical power, the viscous dissipation, the pumping power and the equivalent pressure drop, (b) the mass flow rate, (c) the global heat transfer coefficient, and (d) the merit factor (j/f) for corrugated moving, static with and without lateral damping. The data are presented for different imposed pressure differences for relative amplitude of 89% and $f_r = 50$ Hz.

Table 2
Performances of the dynamic corrugated heat exchanger. Presentation of various global heat transfer and flow properties (when $\Delta P_s > 0$). Pumping power, mechanical power, viscous dissipation, equivalent pressure drop, and merit factor are also presented.

Positive pressure difference, ΔP_s (Pa)	Heat transfer coefficient $(W.m^{-2}.K^{-1})$	Mass flow rate, ρQ_v (kg/s)	Pressure gain, $\Delta P_g = P_2 - P_1 (Pa)$	Pumping power, $P_p = Q_v.\Delta P_g$ (W)	Mechanical power W_p (W)	Viscous dissipation, $W_F(W)$	Equivalent pressure drop, $\Delta P_d (Pa)$	$\frac{j}{f}(-)$
50	8129.00	2.35E-02	676.05	1.59E-02	2.86E-02	1.27E-02	539.38	1.426
100	8096.60	2.34E-02	718.42	1.68E-02	2.98E-02	1.29E-02	552.81	1.381
500	8022.97	2.27E-02	1075.47	2.45E-02	3.87E-02	1.42E-02	625.68	1.175
1000	7928.47	2.20E-02	1531.35	3.37E-02	5.03E-02	1.66E-02	755.89	0.929
5000	7456.99	1.74E-02	5276.14	9.18E-02	1.45E-01	5.28E-02	3036.29	0.172
10000	8632.59	1.35E-02	9957.09	1.34E-01	2.63E-01	1.29E-01	9538.39	0.049

After the evaluation of performances of the same heat exchanger using two different imposed positive pressure differences ($\Delta P_s > 0$), it is thus important to know the limits of direct and reverse flow in the hydraulic circuit. This way of determining fluid flow direction in the exchanger would allow us to capitalize necessary pumping effect to assimilate additional pressure drop in external circuit of the heat exchanger. Such an analysis of determining minimal amplitude (Minimal amplitude$= (A - A_0)/(A_{max} - A_0)$ where A is the used amplitude, A_0 is the amplitude for zero mass flow rate and A_{max} is the maximum amplitude i.e. 100%) as a function of positive pressure difference is presented in Fig. 13.

From the present study, it has been found out that dynamic deformation of the upper wall at lower amplitudes does not produce any pumping effect even if the pressure difference is very low. The higher the pressure difference value is, the more is the possibilities of fluid to be in reverse direction in the exchanger for the amplitudes lower than 80%. This suggests that the device is not able to produce significant pumping power. Either the momentum transmitted to the fluid in such conditions stays low or the viscous

Table 3
Performances of the static corrugated heat exchanger. Presentation of various global heat transfer, flow properties and merit factor.

Positive pressure difference, $\Delta P_s(Pa)$	Equivalent pressure drop, $\Delta P_d(Pa)$	Static corrugated channel with lateral damping			Static corrugated channel without lateral damping		
		Heat transfer coefficient $(W.m^{-2}.K^{-1})$	Mass flow rate, $\rho Q_v(kg/s)$	$\frac{j}{f}(-)$	Heat transfer coefficient $(W.m^{-2}.K^{-1})$	Mass flow rate, $\rho Q_v(kg/s)$	$\frac{j}{f}(-)$
50	539.38	2091.94	1.70E-03	2.656E-02	2609.486	6.31E-04	1.232E-02
100	552.81	2106.46	1.72E-03	2.649E-02	2621.472	6.55E-04	1.253E-02
500	625.68	2184.86	1.86E-03	2.623E-02	2686.254	7.84E-04	1.358E-02
1000	755.89	2323.62	2.11E-03	2.614E-02	2801.166	1.01E-03	1.514E-02
5000	3036.29	4471.33	6.06E-03	3.597E-02	4635.211	4.54E-03	2.794E-02
10000	9538.39	7662.84	1.36E-02	4.395E-02	8011.447	9.63E-03	3.263E-02

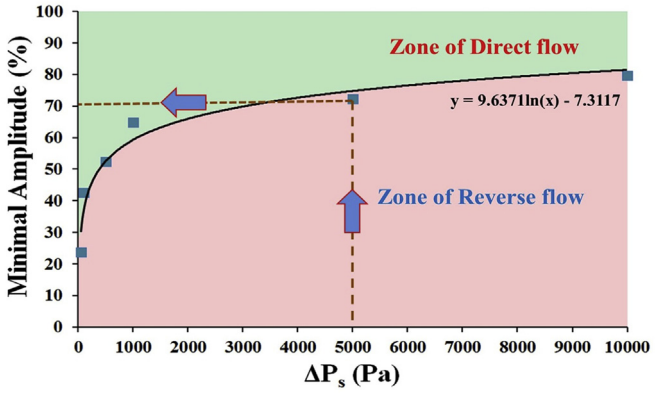

Fig. 13. Zones of direct and reverse flows. Critical limits curve of direct and reverse flows as a function of ΔP_s in the hydraulic circuit for the studied dynamic channel. Note that this presentation is shown for $f_r = 50$ Hz.

dissipation dominates. In this case ($W_F > P_P$), an external pump is needed for the fluid movement in the device for such reverse flows (see also Fig. 11). This would increase overall input power given to the system which would lower down the overall performance. On the other hand, the possibility of fluid to be always in desired direction (direct flow) of hydraulic circuit due to pumping effect when the positive pressure difference is small ($50 < \Delta P_s < 1000$) in the amplitude range of 65%. Importantly, direct flow in the heat exchanger can always be achieved at higher amplitudes ($A > 80\%$) irrespective of any value of imposed pressure difference. For a given thermo-hydraulic constraint, minimal amplitude can be easily obtained using the simple mathematical expression presented in Fig. 13 where fluid flow direction in the exchanger can be evaluated using two different zones.

5. Conclusion

A new concept of heat exchanger at millimeter scale is proposed that consists in dynamically deforming one of the walls. The proposed system at miniature scale is capable of performing extremely well in low Reynolds number range (up to $Re = 600$) contrary to existing systems. The enhancement in heat transfer and mass flow rate as a function of imposed pressure differences were investigated in single-phase flow. It was observed that the heat transfer coefficient and mass flow rate increases with increase in amplitude when positive pressure difference was applied. The current results show that the requirement of external pump could be completely eliminated and thus, increasing the overall performance of the system. The system performance is always significantly high while it starts to deteriorate at high imposed positive difference and tends to reach the similar performances of static corrugated and straight channels. Based on the operating and mechanical constraints, the performance of the proposed millimeter scale heat exchanger can be easily exploited and thus, a substantial gain in terms of integration can be achieved.

Acknowledgement

The authors would like to thank the financial support from Fonds Unique Interministériel (Grant FUI18-CANOPEE) obtained in the framework of CANOPÉE (Contrôle Actif d'un draiN à calOries pour l'Electronique Embarquée) project.

Nomenclature

A	Relative amplitude $(-)$
C_p	Volumetric thermal capacity $(J.m^{-3}.K^{-1})$
D_h	Hydraulic diameter (m)
f_r	Frequency (Hz)
f	Friction factor based on pressure drop, $\Delta P_d < 0$ $(-)$
h	Mean heat transfer coefficient at the heated wall $(W.m^{-2}.K^{-1})$
h	Global heat transfer coefficient at the heated wall $(W.m^{-2}.K^{-1})$
j	Colburn factor $(-)$
k_f	Thermal conductivity of fluid $(W.m^{-1}.K^{-1})$
Pr	Prandtl number $(-)$
L	Imprint length of heated zone (m)
$\dot{m}$	Mass flow rate $(kg.s^{-1})$
Nu	Mean Nusselt number $(-)$
Nu	Global Nusselt number $(-)$
q	Heat Flux $(W.m^{-2})$
Q_v	Volumetric mass flow rate $(m^3.s^{-1})$
ΔP_d	Equivalent pressure drop in actuated zone (Pa)
ΔP_g	Pressure gain in actuated zone (Pa)
ΔP_s	Pressure difference between outlet-inlet sections (Pa)
P_P	Pumping power (W)
p	Perimeter of the channel passage (m)
S	Exchange surface (m^2)
t	Time (s)
$\overline{T}_{fm}$	Mean fluid temperature at a given axial position in the channel (K)
$\overline{T}_{fm}$	Mean fluid temperature in the channel (K)

$\overline{T}_w$ Mean wall temperature on a heated zone position in the actuated zone (K)
$\overline{\overline{T}}_w$ Mean wall temperature in the actuated zone (K)
$\vec{u}$ Average velocity ($m.s^{-1}$)
V Volume of channel (m^3)
W Channel width (m)
W_F Viscous dissipation (W)
W_P Mechanical power (W)

Greek symbols
δ Average distance between walls (m)
ρ Density ($kg.m^{-3}$)
λ Wavelength (m)
Γ Imposed power (W)
ω Number of waves per unit length (m^{-1})
Y_1 and Y_2 Threshold functions (–, Eq. (4))
μ Dynamic viscosity ($kg.m^{-1}.s^{-1}$)
τ Period (s^{-1})

References

[1] Mohan N, Underland TM, Robbins WP. Power electronics, converters, applications, and design. third ed. John Wiley & Sons, Inc; 2003. p. 730–42.
[2] Kandlikar SG. Heat transfer, pressure drop and flow patterns during flow boiling in parallel channel compact heat exchangers of small hydraulic diameters. Heat Transf Eng 2001;23(No. 5):5–23.
[3] Kandlikar SG. Fundamental issues related to flow boiling in minichannels and microchannels, experimental heat transfer, fluid mechanics and thermodynamics. In: Proceedings of the Fifth World Conference on Experimental Heat Transfer, Fluid Mechanics, and Thermodynamics, Thessaloniki, Greece, Sept, vol. 1; 2001. p. 129–46.
[4] Sunden B, Trollheden S. Periodic laminar flow and heat transfer in a corrugated two-dimensional channel. Int Comm Heat Mass Transf 1989;16:215–25.
[5] Kanaris AG, Mouza AA, Paras SV. Flow and heat transfer in narrow channels with corrugated walls. Chem Eng Res Des 2005;83:460–8.
[6] Naphon P. Effect of wavy plate geometry configurations on the temperature and flow distributions. Int Comm Heat Mass Transf 2009;36:942–6.
[7] Zhang C, Chen Y, Shi M. Effects of roughness elements on laminar flow and heat transfer in microchannels. Chem Eng Process 2010;49:1188–92.
[8] Mohammed HA, Abed AM, Wahid MA. The effects of geometrical parameters of a corrugated channel with in out-of-phase arrangement. Int Comm Heat Mass Transf 2013;40:47–57.
[9] Léal L, Miscevic M, Lavieille P, Amokrane M, Pigache F, Topin F, et al. An overview of heat transfer enhancement methods and new perspectives: focus on active methods using electroactive materials. Int J Heat Mass Transf 2013;61:505–24.
[10] Nakamura M, Nakamura T, Tanaka T. A computational study of viscous flow in a transversally oscillating channel. JSME Int J Ser C Mech Syst Mach Elem Manuf 2000;43(4):837–44.
[11] Comini G, Nonino C, Savino S. Effect of space ratio and corrugation angle on convection enhancement in wavy channels. Int J Num Methods Heat Fluid Flow 2002;13(4):500–19.
[12] Hossain MZ, Islam AKMS. Fully developed flow structures and heat transfer in sine-shaped wavy channels. Int Comm Heat Mas Transf 2004;31(6):887–96.
[13] Kumar P, Topin F, Miscevic M, Lavieille P, Tadrist L. Numerical heat and mass transfer in porous media. Adv Struct Mater. 2012;27:181–208.
[14] Léal L, Topin F, Lavieille P, Tadrist L, Miscevic M. Simultaneous integration, control and enhancement of both fluid flow and heat transfer in small scale heat exchangers: a numerical study. Int Commun Heat Mass Transf 2013;49:36–40.
[15] http://mdx.plm.automation.siemens.com/star-ccm-plus.
[16] Lee P-S, Garimella SV, Liu D. Investigation of heat transfer in rectangular microchannels. Int J Heat Mass Transf 2005;48:1688–704.
[17] Faghri A, Zhang Y, Howell J. Advanced heat and mass transfer. Columbia, MO: Global Digital Press; 2010.
[18] Kuppan T. Heat exchanger design book. New York: Marcel Dekker Inc; 2000.